LETTER

doi:10.1038/nature20826

Onset of the aerobic nitrogen cycle during the Great Oxidation Event

Aubrey L. Zerkle[1], Simon W. Poulton[2], Robert J. Newton[2], Colin Mettam[1], Mark W. Claire[1,3], Andrey Bekker[4] & Christopher K. Junium[5]

The rise of oxygen on the early Earth (about 2.4 billion years ago)[1] caused a reorganization of marine nutrient cycles[2,3], including that of nitrogen, which is important for controlling global primary productivity. However, current geochemical records[4] lack the temporal resolution to address the nature and timing of the biogeochemical response to oxygenation directly. Here we couple records of ocean redox chemistry with nitrogen isotope ($^{15}N/^{14}N$) values from approximately 2.31-billion-year-old shales[5] of the Rooihoogte and Timeball Hill formations in South Africa, deposited during the early stages of the first rise in atmospheric oxygen on the Earth (the Great Oxidation Event)[6]. Our data fill a gap of about 400 million years in the temporal $^{15}N/^{14}N$ record[4] and provide evidence for the emergence of a pervasive aerobic marine nitrogen cycle. The interpretation of our nitrogen isotope data in the context of iron speciation and carbon isotope data suggests biogeochemical cycling across a dynamic redox boundary, with primary productivity fuelled by chemoautotrophic production and a nitrogen cycle dominated by nitrogen loss processes using newly available marine oxidants. This chemostratigraphic trend constrains the onset of widespread nitrate availability associated with ocean oxygenation. The rise of marine nitrate could have allowed for the rapid diversification and proliferation of nitrate-using cyanobacteria and, potentially, eukaryotic phytoplankton.

Nitrogen (N) is an essential element for all living organisms, required alongside carbon (C) and phosphorus (P) for the formation of nucleic acids and proteins. As a result, N and P are the principal limiting nutrients controlling autotrophic CO_2 fixation, which in turn regulates climate, weathering, and the redox state of Earth's surface on geologic timescales.

The marine nitrogen cycle is driven largely by biological processes. The primary source of N to the biosphere is nitrogen fixation, the conversion of atmospheric N_2 to organic nitrogen in its bioavailable form (ammonium, NH_4^+). In the modern oceans, ammonium is oxidized via the stepwise process of nitrification, producing nitrite (NO_2^-) and nitrate (NO_3^-). Nitrate (and nitrite) can be assimilated into organic matter, by both oxygenic photoautotrophic bacteria (cyanobacteria) and eukaryotic phytoplankton. Fixed nitrogen is mostly recycled in the water column, but some sinks to the sediments where it is buried and/or remineralized. Some bioavailable nitrogen in the modern oceans is returned to the atmosphere as N_2 via denitrification (the reduction of nitrate) and anaerobic ammonium oxidation (anammox, the oxidation of ammonium with nitrite) in oxygen-minimum zones[7].

Each of these transformations can affect the ratio of nitrogen isotopes ($\delta^{15}N = (^{15}N/^{14}N)_{sample}/(^{15}N/^{14}N)_{atmospheric\ N2} - 1$, measured in per mil, ‰), producing fractionations between reactant and product N species[8]. Nitrogen fixation produces small negative fractionations from atmospheric N_2, resulting in organic $\delta^{15}N$ values[9] of −4‰ to 0‰. Denitrification and anammox preferentially return the lighter isotope to the atmosphere, leaving the residual nitrate and nitrite enriched[8,10] in ^{15}N by 10‰–25‰. Large fractionations can also be produced by nitrification and biological assimilation[11] (and possibly by dissimilatory nitrate reduction to ammonium[12]). However, these fractionations are not expressed in most modern environments, since nitrification and the recycling of fixed N compounds occur rapidly and nearly quantitatively. Hence, nitrogen loss via denitrification and anammox dominates the modern nitrogen isotope signal, resulting in sedimentary organic matter with average $\delta^{15}N$ values[13] of 7‰, owing to the uptake of ^{15}N-enriched residual nitrate by primary producers.

Beaumont and Robert[2] were the first to suggest a secular trend in the nitrogen isotope values of organic N for Archean and early Proterozoic sediments. They noted that the $\delta^{15}N$ of kerogen in Archean cherts centred at about 0‰ (ranging from −6‰ to +13‰), while the $\delta^{15}N$ of early

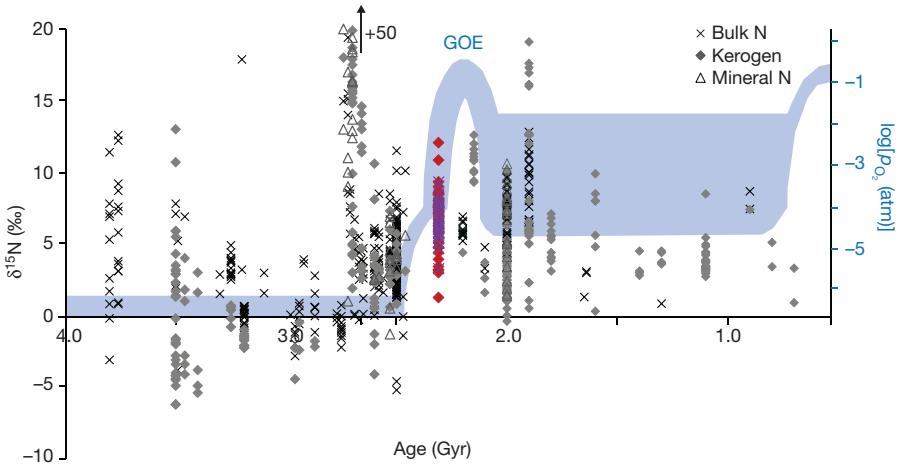

Figure 1 | Secular trend in sedimentary $\delta^{15}N$ over early Earth history. Data are from ref. 29, and the references listed therein. 'Mineral N' refers to nitrogen extracted as ammonium from phyllosilicates. Red and purple data points are from this study, denoting kerogen and bulk rock analyses, respectively. Errors are within the size of the symbols. Shown in blue is the current view on atmospheric O_2 content (p_{O_2}), adapted from ref. 30, and the approximate timing of the Great Oxidation Event (GOE).

[1]School of Earth and Environmental Sciences and Centre for Exoplanet Science, University of St Andrews, St Andrews KY16 9AL, UK. [2]School of Earth and Environment, University of Leeds, Leeds LS2 9JT, UK. [3]Blue Marble Space Institute of Science, PO Box 88561, Seattle, Washington 98145, USA. [4]Department of Earth Sciences, University of California-Riverside, Riverside, California 92521, USA. [5]Department of Earth Sciences, Syracuse University, Syracuse, New York 13244, USA.

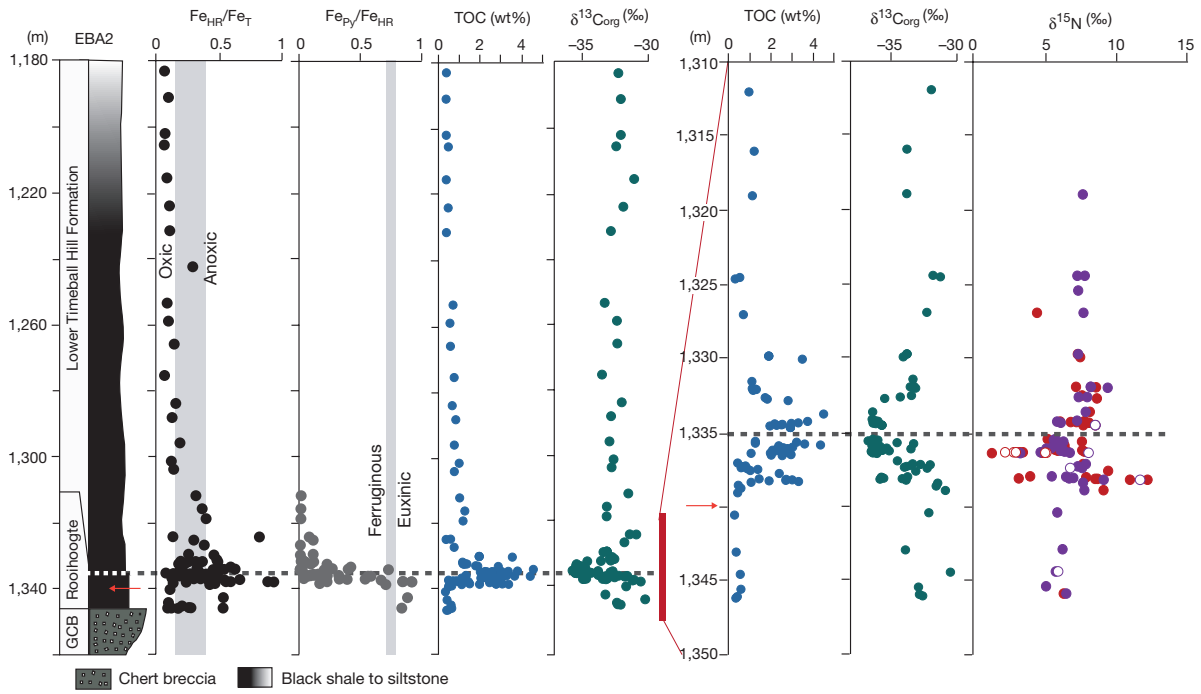

Figure 2 | Lithological and geochemical data for core EBA-2. The Rooihoogte and Timeball Hill formations are shown, overlying the Great Chert Breccia (GCB), which developed at the top of the Malmani carbonate platform. Data include Fe speciation, total organic carbon (TOC), and $\delta^{13}C_{org}$ spanning the section. Fe_{Py}/Fe_{HR} data are only shown for samples having Fe_{HR}/Fe_T values that suggest anoxic deposition. The inset is a blow-up of $\delta^{15}N$ values, alongside TOC and $\delta^{13}C_{org}$, for the boundary of the Rooihoogte and Timeball Hill formations (red bar). For $\delta^{15}N$, red data points are extracted kerogen, purple data points are bulk rock N, and empty symbols were measured using a nano-elemental analyser technique. For all data, errors are within the size of the symbols. The orange arrows denote the disappearance of mass-independent fractionation of sulfur isotopes in drill core EBA-2 (ref. 6).

Proterozoic kerogens centred at about 5‰, with a total range similar to that in Phanerozoic sediments (about 0‰ to 10‰) (Fig. 1). Our statistical treatment of the temporal $\delta^{15}N$ record (Extended Data Fig. 1) alongside more recent compilations[14] supports this shift, which occurs broadly coeval with the Great Oxidation Event (GOE) from 2.45–2.32 billion years (Gyr) ago[1,15], although its precise timing remains poorly constrained. As such, the secular rise in $\delta^{15}N$ is commonly interpreted to reflect the transition from an anaerobic nitrogen cycle dominated by reduced N species (N_2 and ammonium), to a modern-style aerobic nitrogen cycle with nitrate as a sizeable component of dissolved inorganic nitrogen. Small (about 2‰ to 5‰) positive excursions in $\delta^{15}N$ within older (around 2.6–2.5 Gyr old) sedimentary rocks have been interpreted to represent the temporary onsets of nitrification/denitrification during transient or localized oxygenation events, which were apparently not sufficiently widespread or long-lived for the signal to persist[16,17]. Alternatively, these small and short-lived positive shifts in $\delta^{15}N$ recorded exclusively in deep-water facies could reflect the incorporation of ^{15}N-enriched ammonium produced by partial nitrification, assimilation of ^{15}N-depleted ammonium in shallow waters, or nitrogen redox cycling independent of surface oxygenation[4,18,19]. However, no records of contemporaneous shallow-water sediments linked directly to records of ocean or atmospheric oxygenation have so far been available to test these alternatives.

Here we examine the response of the nitrogen cycle to changing atmosphere and ocean redox conditions during the deposition of approximately 2.31-Gyr-old siliciclastic rocks, filling a gap of about 400 million years in the temporal $\delta^{15}N$ record (Fig. 1), in sediments contemporaneous with the early stages of the GOE. We focus our analyses on the Rooihoogte and Timeball Hill formations, present in drill core EBA-2 in the Potchefstroom Synclinorium, South Africa (Extended Data Figs 2 and 3). The Rooihoogte and Timeball Hill formations form the basal part of the Pretoria Group in the Transvaal basin, and were deposited on a palaeo-delta slope open to the ocean[1]. U–Pb zircon ages for the tuffs in the lower Timeball Hill formation give an age[5] of 2.310 ± 0.009 Gyr. Atmospheric oxygen content is constrained by the transition from mass-independent to mass-dependent fractionation of sulfur isotopes recently placed within shales of the Rooihoogte Formation[6] (Fig. 2), indicating a rise in atmospheric O_2 levels to greater than one part per million[20]. $\delta^{34}S$ data for sedimentary sulfides in the Rooihoogte and Timeball Hill formations also indicate a notable rise in seawater sulfate[1,6], consistent with an increase in oxidative weathering of sulfide minerals on the continents. Additional sample information and discussion of post-depositional alteration is available in Methods and Extended Data Figs 4 and 5.

We used a well established sequential iron extraction technique[21] (the ratio of highly reactive to total Fe, Fe_{HR}/Fe_T, and the ratio of Fe in pyrite to highly reactive Fe, Fe_{Py}/Fe_{HR}) to assess the redox state of the water column during deposition of the Rooihoogte and Timeball Hill formations. Large variations in iron speciation indicate highly dynamic seawater redox conditions during deposition of the Rooihoogte formation and the lower 20 m or so of the Timeball Hill formation (Fig. 2), with fluctuations between oxic, ferruginous (anoxic and Fe(II)-rich), and euxinic (anoxic and sulfide-rich) states. The rapid changes in water-column chemistry suggest that deposition occurred close to a redox interface (chemocline) between oxygenated surface waters and anoxic deep waters that were episodically driven euxinic, possibly by variations in organic carbon delivery or seawater sulfate availability. These data also imply the existence of a transiently sulfidic shelf underlying an oxygenated surface ocean, similar to the redox stratification suggested for the late Archean[22]. Fluctuations in Fe speciation records are accompanied by a significant increase in total organic carbon (from <1% to about 4%) and a decrease in $\delta^{13}C_{org}$ (from −32‰ to −36‰) across the boundary of the Rooihoogte and Timeball Hill formations (Fig. 2), consistent with chemoautotrophic carbon fixation at or near a chemocline[23].

The $\delta^{15}N$ values for both bulk nitrogen, $\delta^{15}N_{bulk}$, and extracted kerogen, $\delta^{15}N_{org}$, show a high degree of variability across this same interval (Fig. 2). When interpreted within the context of the

Fe speciation data, these values are consistent with a marine nitrogen cycle developed across a dynamic redox boundary. $\delta^{15}N$ values of $6.0‰ \pm 0.5‰$ in the lower part of the section are similar to those of modern marine organic matter[13], which reflect a nitrogen cycle dominated by N loss via denitrification and anammox in oxygen minimum zones[24]. Nitrogen isotope values vary from 1.4‰ to 12‰ across the boundary between the Rooihoogte and Timeball Hill formations, consistent with a variable input from similar chemotrophic communities across a shifting redox interface. These changes could reflect imbalances in ammonium supply and nitrification–denitrification resulting from periodic upwelling of nutrients and high organic productivity. On a stratified Paleoproterozoic marine shelf, uptake of ammonium from anoxic deep waters would have produced ^{15}N-depleted biomass just below the chemocline. Nitrification with newly available marine oxidants would have further enriched residual ammonium in ^{15}N across the redox interface. Higher $\delta^{15}N$ in oxygenated shallow waters could result from the uptake of this ^{15}N-enriched ammonium, or by nitrate assimilation once nitrate levels had risen high enough to support partial denitrification. The $\delta^{15}N$ stabilizes at near-modern values ($7.2‰ \pm 1.0‰$) up-section in the lower Timeball Hill formation, in association with Fe-speciation data indicative of the onset of pervasively oxygenated shallower water conditions. Oxygenation of surface waters would have supported widespread nitrification and further enhanced nitrate availability.

Notably, within the context of the global $\delta^{15}N$ record (Fig. 1), the succession of the Rooihoogte and Timeball Hill formations records the first clear evidence for a long-lived aerobic nitrogen cycle in the sedimentary record. The approximately 2.31-Gyr-old section of the Rooihoogte and Timeball Hill formations, deposited at the heart of the GOE and coincident with the permanent loss of mass-independent S-isotope fractionation[6], is bracketed by evidence for only transient aerobic nitrogen cycling in older sediments (from around 2.7–2.5 Gyr ago[16,17,19]), and the clear isotopic imprint of aerobic nitrogen cycling in records from younger sediments deposited after approximately 2.0 Gyr ago[25–28], as confirmed by statistical analysis of the global database (Extended Data Fig. 1). Available data suggests that earlier transient oxygenation events were insufficient to establish the modern nitrogen cycle, because marine nitrate was not pervasive in the oceans before the GOE[16,17]. In addition, $\delta^{15}N$ values $>2‰$ are typical for the remainder of the Precambrian record (Fig. 1), indicating that aerobic nitrogen cycling became at least locally widespread enough to impart a long-lived isotopic imprint on marine $\delta^{15}N$ during the GOE.

The build-up of a substantial marine nitrate reservoir would have provided an important evolutionary driver, because prokaryotes and eukaryotic phytoplankton that were able to utilize nitrate as a primary nutrient source could have diversified to fill this new ecological niche. The co-occurrence of this event with other geochemical changes indicative of a pervasive oxygenation of Earth's atmosphere provides a crucial constraint on the surprisingly rapid response time of the global biosphere to this major transition in Earth's surface chemistry.

Online Content Methods, along with any additional Extended Data display items and Source Data, are available in the online version of the paper; references unique to these sections appear only in the online paper.

Received 22 May 2013; accepted 18 November 2016.
Published online 6 February 2017.

1. Bekker, A. *et al.* Dating the rise of atmospheric oxygen. *Nature* **427,** 117–120 (2004).
2. Beaumont, V. & Robert, F. Nitrogen isotope ratios of kerogens in Precambrian cherts: a record of the evolution of atmosphere chemistry? *Precambr. Res.* **96,** 63–82 (1999).
3. Bekker, A. & Holland, H. D. Oxygen overshoot and recovery during the early Paleoproterozoic. *Earth Planet. Sci. Lett.* **317–318,** 295–304 (2012).
4. Stüeken, E. E., Kipp, M. A., Koehler, M. C. & Buick, R. The evolution of Earth's biogeochemical nitrogen cycle. *Earth Sci. Rev.* **160,** 220–239 (2016).
5. Rasmussen, B., Bekker, A. & Fletcher, I. R. Correlations of Paleoproterozoic glaciations based on U-Pb zircon ages for tuff beds in the Transvaal and Huronian Supergroups. *Earth Planet. Sci. Lett.* **382,** 173–180 (2013).
6. Luo, G. *et al.* Rapid oxygenation of Earth's atmosphere 2.33 billion years ago. *Sci. Adv.* **2,** e1600134 (2016).
7. Dalsgaard, T., Thamdrup, B., Farias, L. & Revsbech, N. P. Anammox and denitrification in the oxygen minimum zone of the eastern South Pacific. *Limnol. Oceanogr.* **57,** 1331–1346 (2012).
8. Wada, E. in *Isotope Marine Chemistry* (eds Goldberg, E. D., Horibe, Y. & Saruhashi, K.) 375–398 (Uchida Rokakuho, 1980).
9. Zerkle, A. L., Junium, C. K., Canfield, D. E. & House, C. H. Production of ^{15}N-depleted biomass during cyanobacterial N_2-fixation at high Fe concentrations. *J. Geophys. Res.* **113,** G03014 (2008).
10. Brunner, B. *et al.* Nitrogen isotope effects induced by anammox bacteria. *Proc. Natl Acad. Sci. USA* **110,** 18994–18999 (2013).
11. Hoch, M. P., Fogel, M. L. & Kirchman, D. L. Isotope fractionation associated with ammonium uptake by a marine bacterium. *Limnol. Oceanogr.* **37,** 1447–1459 (1992).
12. McCready, R. G. L., Gould, W. D. & Barendregt, R. W. Nitrogen isotope fractionation during the reduction of NO_3^- to NH_4^+ by *Desulfovibrio* sp. *Can. J. Microbiol.* **29,** 231–234 (1983).
13. Peters, K. E., Sweeney, R. E. & Kaplan, I. R. Correlation of carbon and nitrogen stable isotope ratios in sedimentary organic matter. *Limnol. Oceanogr.* **23,** 598–604 (1978).
14. Ader, M. *et al.* Interpretation of the nitrogen isotopic composition of Precambrian sedimentary rocks: assumptions and perspectives. *Chem. Geol.* **429,** 93–110 (2016).
15. Farquhar, J., Zerkle, A. L. & Bekker, A. Geological constraints on the origin of oxygenic photosynthesis. *Photosynth. Res.* **107,** 11–36 (2011).
16. Garvin, J., Buick, R., Anbar, A. D., Arnold, G. L. & Kaufman, A. J. Isotopic evidence for an aerobic nitrogen cycle in the latest Archean. *Science* **323,** 1045–1048 (2009).
17. Godfrey, L. V. & Falkowski, P. G. The cycling and redox state of nitrogen in the Archaean ocean. *Nat. Geosci.* **2,** 735–729 (2009).
18. Thomazo, C., Ader, M. & Philippot, P. Extreme ^{15}N-enrichments in 2.72-Gyr-old sediments: evidence for a turning point in the nitrogen cycle. *Geobiology* **9,** 107–120 (2011).
19. Busigny, V., Lebeau, O., Ader, M., Krapez, B. & Bekker, A. Nitrogen cycle in the Late Archean ferruginous ocean. *Chem. Geol.* **362,** 115–130 (2013).
20. Pavlov, A. A. & Kasting, J. F. Mass-independent fractionation of sulfur isotopes in Archean sediments: strong evidence for an anoxic Archean atmosphere. *Astrobiology* **2,** 27–41 (2002).
21. Poulton, S. W. & Canfield, D. E. Development of a sequential extraction procedure for iron: implications for iron partitioning in continentally derived particulates. *Chem. Geol.* **214,** 209–221 (2005).
22. Reinhard, C. T., Raiswell, R., Scott, C., Anbar, A. D. & Lyons, T. W. A late Archean sulfidic sea stimulated by early oxidative weathering of the continents. *Science* **326,** 713–716 (2009).
23. Coetzee, L. L., Beukes, N. J., Gutzmer, J. & Kakegawa, T. Links of organic carbon cycling and burial to depositional depth gradients and establishment of a snowball Earth at 2.3Ga. Evidence from the Timeball Hill Formation, Transvaal Supergroup, South Africa. *S. Afr. J. Geol.* **109,** 109–122 (2006).
24. De Pol-Holz, R., Robinson, R. S., Hebbeln, D., Sigman, D. M. & Ulloa, O. Controls on sedimentary nitrogen isotopes along the Chile margin. *Deep-Sea Res. II* **56,** 1042–1054 (2009).
25. Godfrey, L. V., Poulton, S. W., Bebout, G. E. & Fralick, P. W. Stability of the nitrogen cycle during development of sulfidic water in the redox-stratified late Paleoproterozoic Ocean. *Geology* **41,** 655–658 (2013).
26. Stüeken, E. E. A test of the nitrogen-limitation hypothesis for retarded eukaryote radiation: nitrogen isotopes across a Mesoproterozoic basinal profile. *Geochim. Cosmochim. Acta* **120,** 121–139 (2013).
27. Papineau, D. *et al.* High primary productivity and nitrogen cycling after the Paleoproterozoic phosphogenic event in the Aravalli Supergroup, India. *Precambr. Res.* **171,** 37–56 (2009).
28. Kump, L. R. *et al.* Isotopic evidence for massive oxidation of organic matter following the Great Oxidation Event. *Science* **334,** 1694–1696 (2011).
29. Farquhar, J., Zerkle, A. L. & Bekker, A. in *Treatise in Geochemistry: Reference Module in Earth Systems and Environmental Sciences* (eds Holland, H. D. & Turekian, K.) Vol. 6, 91–138 (Elsevier, 2014).
30. Lyons, T. W., Reinhard, C. T. & Planavsky, N. J. The rise of oxygen in Earth's early ocean and atmosphere. *Nature* **506,** 307–315 (2014).

Acknowledgements This study was supported financially by a Natural Environment Research Council Fellowship (number NE/H016805 to A.L.Z.). We thank the Council for Geoscience in South Africa and the staff at the National Core Library in Donkerhoek for facilitating access to the core materials, and M. Yun for assistance with stable isotope analyses at the University of Manitoba.

Author Contributions A.L.Z. and S.W.P. conceived the study. S.W.P. and A.B. collected the samples. A.L.Z., S.W.P., R.J.N., C.M. and C.K.J. processed samples and performed geochemical analyses. M.W.C. provided statistical analyses of the global database. A.L.Z. interpreted the data and wrote the manuscript with input from all coauthors.

Author Information Reprints and permissions information is available at www.nature.com/reprints. The authors declare no competing financial interests. Readers are welcome to comment on the online version of the paper. Correspondence and requests for materials should be addressed to A.Z. (az29@st-andrews.ac.uk).

METHODS

Statistical analysis of $\delta^{15}N$ database. Previous studies have used age-binned means of the $\delta^{15}N$ database over hand-picked geologic intervals to propose changes in this proxy with time[2,4,14,31]. These studies have provided a qualitative indication that the $\delta^{15}N$ record appears to vary systematically over geologic time. However, they are not statistically robust, because two samples drawn from a single population will often express different means owing to random noise. A Student's *t*-test is a more statistically robust method for determining whether two (otherwise normally distributed) sample sets are likely to arise from the same population, which is considered the null hypothesis. We therefore performed 754 independent two-tailed *t*-tests spanning every possible time-weighted binning of the $\delta^{15}N$ database, assuming unequal variances in the sample sets. In all but a few cases at the extremes (where the bin sizes of one of the sample sets were small), the null hypothesis was rejected at greater than 99% confidence and so we can conclude that the divided sample sets arise from populations with different means and variances.

The sample sets are defined as ranging from the first database entry from the Proterozoic, at 0.70 Gyr ago, to the entry with the age shown on the horizontal axis of Extended Data Fig. 1, and then from the subsequent entry to our final database entry, with age of 3.80 Gyr. Extended Data Fig. 1 shows the logarithm of the 'false-positive' probability that the two samples sets arise from populations of the same mean and variance. Using this method, datasets from 2.31 Gyr ago (this study), 2.50 Gyr ago and 2.70–2.80 Gyr ago are demonstrated to be the most statistically meaningful pivot ages (pivot ages separate the database into distinct sample sets).

As discussed in the main text, the large number of database entries from about 2.50 Gyr ago stem from predominantly deep-water environments that show small stratigraphic shifts in $\delta^{15}N$, interpreted to reflect temporary localized nitrification/denitrification in an otherwise reducing ocean[16,17,19]. As a result, the global database may be slightly biased towards results showing an 'oxic' nitrogen cycle at this time period. The data presented in this study are from unequivocally oxic shallow waters, and the statistical analysis confirms that our new data provide a stronger statistical power in separating the datasets, even given the bias in the database at 2.50 Gyr ago. As we note in the main text, additional $\delta^{15}N$ data from shallow-water depositional environments in this crucial interval are required to test alternative hypotheses.

Although it is beyond the scope of this current study, we additionally note that the most statistically meaningful separation of the $\delta^{15}N$ database occurs when the sample sets are split into the time periods 0.70–2.71 Gyr ago and 2.75–3.80 Gyr ago. The statistical power for this split is driven primarily by the predominance of extremely ^{15}N-enriched $\delta^{15}N$ measurements (upwards of +55‰, dominantly in kerogens) from this time period. The origin of these extreme values is highly debated, with hypotheses including the onset of partial nitrification[18], and effects from ammonia degassing under highly alkaline conditions[32]. Regardless, it is clear that the data from around 2.70 Gyr ago do not represent a modern-style aerobic N cycle, as no such extreme values are seen anywhere in the modern Earth system. These statistical analyses therefore demonstrate that the nitrogen cycle underwent massive changes in both the early Neoarchean[4] and at the GOE, with the data from this study forming the key pivot point for the latter.

Fe and C analyses. Iron speciation was determined by means of the sequential extraction technique described in ref. 21, with a relative standard deviation of <5% for all extraction steps. TOC was measured on a Leco analyser after decarbonation by treatment with 20% HCl, with a 1σ of 0.05%. $\delta^{13}C_{org}$ was measured at the SIFIR Laboratory at the University of Manitoba. A calibration line was calculated by least-squares linear regression of analyses of two international standards (USGS40, USGS41) performed at the beginning, middle and end of each run. Replicate analyses of international standard USGS Green River shale SGR-1b ($\delta^{13}C_{org} = -29.3 \pm 0.1$‰ VPDB) alongside unknown samples yielded $\delta^{13}C_{org} = -29.5 \pm 0.2$‰ ($n = 29$).

Kerogen N-isotope analyses. Kerogen was extracted following a method modified from ref. 33 in the Geobiology laboratory at the University of St Andrews. Approximately 100–200 mg of bulk rock powders were decarbonated twice with 10% (v/v) HCl overnight at 40 °C in a clean hood, then transferred to Teflon beakers in a dedicated fume cupboard, where 5 ml of 10% HCl + 2 ml of concentrated HF was added and volatilized at 40 °C. Residues were rinsed five times with Milli-Q water. Chloroform was added to the residue, shaken, and allowed to settle in separation funnels for about 30 min. Heavy minerals that sank to the bottom were first removed, and then floated kerogen was transferred to a Teflon beaker, dried in a clean hood, and stored in an anaerobic chamber until analysis. A subset of samples were also extracted commercially at Global Geolab Ltd, using techniques similar to those above, except that kerogens were separated out by heavy liquid separation with zinc bromide instead of chloroform. Repeat extracts of the same sample (all plotted in Fig. 2) had consistent $\delta^{15}N_{org}$ values between laboratories, generally within 1‰ (see Source Data for Fig. 2).

Kerogen N isotope ratios ($\delta^{15}N_{org}$) were measured using a Eurovector 3028HT elemental analyser fitted with a Costech Zero Blank autosampler coupled to an Isoprime isotope ratio mass spectrometer, at the University of Leeds. Columns with reagents were fitted to the elemental analyser along with either a high-resolution CN gas chromatography column (Elemental Microanalysis E3037), or a NCH column (Elemental Microanalysis E3001), as below. A magnesium perchlorate-carbosorb trap was used to trap water and CO_2. The setup was leak-checked and then the combustion and reduction furnaces were heated to operating temperatures and left purging with He overnight. The combustion furnace was held at 1,020 °C and the reduction furnace at 650 °C. The gas chromatography column was baked at 190 °C with He flowing overnight, and then its temperature was reduced to the normal running temperature (80 °C for the NCH column, and 110 °C for the high-resolution CN column).

Samples were prepared by weighing between 10 mg and 30 mg of kerogen into 8 mm × 5 mm tin cups. These were loaded into the autosampler and purged for at least an hour before analyses. Upon sealing the autosampler chamber and opening it to the main He flow, mass 28 was monitored until it returned to a stable background (less than 7×10^{-11} nA). Samples were combusted in a pulse of pure oxygen (N5.0 grade, BOC) and injected into a stream of helium (CP grade, BOC). The resulting gases were passed through chromous oxide and silvered cobaltous oxide, fine copper wires, and a magnesium perchlorate/carbosorb trap before entering the gas chromatography column. The mass 29/28 ratio of the sample N_2 gas was measured relative to a pulse of pure N_2 (research grade, BOC) and corrected to the AIR scale (the air standard) using the USGS-25 and USGS-26 ammonium sulfate standards, with $\delta^{15}N_{AIR}$ values of −30.1‰ and +53.7‰, respectively. Repeated runs of standard materials during each analytical session produced standard deviations of the raw $\delta^{15}N_{refgas}$ that were generally between 0.15‰ and 0.41‰, with the majority ≤0.30‰. Data were corrected with bracketing standards using a simple linear regression equation. Repeats of an in-house yeast standard (7.6 wt% N) gave a long-term average value of -0.8 ± 0.31‰ (1σ, 37 runs with both NCH and high-resolution CN gas chromatography columns), with in-run reproducibility always ≤0.2‰ where three or more repeats were measured during the same analytical session. A sample size test using the same yeast standard determined that samples producing peak heights of <1 nA have larger variability, approaching the blank $\delta^{15}N$ value as their peak height decreased. Repeat analyses of the yeast standard with peak height >1 nA produced $\delta^{15}N_{refgas}$ values that differed by ≤0.1‰. Therefore, analyses that produced peak heights of <1 nA were discarded in this study.

The analysis of organic materials with low concentrations of nitrogen can be complicated by the production of CO gas (at masses 28 and 29) as a result of incomplete combustion, which can alter the apparent $^{15}N/^{14}N$ ratio of the sample. We took the following precautions to ensure that data were not affected by CO production during incomplete combustion: (1) combustion tests using a low-N organic material (cornflower, 0.07 wt% N); (2) mass 30 monitoring; and (3) use of an NCH column to produce a better separation between the N_2 and unwanted CO (which might produce a secondary mass 28 peak for samples affected by partial combustion).

Bulk rock analyses. A subset of samples from the Rooihoogte and Timeball Hill formations was analysed for bulk rock geochemistry (wt% K_2O) to screen for post-depositional alteration at the University of St Andrews, using standard X-ray fluorescence (with 1σ of 0.02 wt%). Bulk nitrogen content (% TN) and bulk $\delta^{15}N$ ($\delta^{15}N_{bulk}$, without decarbonation) were measured at the SIFIR Laboratory at the University of Manitoba. Analyses were performed using a Costech 4010 elemental analyser fitted with a Costech Zero Blank autosampler and coupled to a Thermo Finnigan Delta V Plus isotope-ratio mass spectrometer via an open-split interface (ConFlo III, Thermo Finnigan). A magnesium perchlorate-carbosorb trap was placed before the ConFlo III to remove remaining water and CO_2. To improve the efficiency of sample combustion, temperature in the oxidation column was raised to 1,050 °C, and a 'macro' O_2 injection loop was used. The setup was leak-checked and then the oxidation and reduction columns were heated to operating temperatures and left purging with He overnight. The oxidation column was held at 1,050 °C and the reduction column at 650 °C. The approximately 3-m-long stainless steel gas chromatography column was baked at 100–110 °C with He flowing overnight, and then its temperature was reduced to the normal running temperature (55 °C). CO_2 level was monitored during analytical sessions. Sample normalization was performed using the two-point calibration described in ref. 34, by analysing two international standards (USGS40 and USGS41) at the beginning, middle and end of each analytical session. Two certified standards were additionally analysed alongside with samples: B2153, soil, % TN = 0.13 ± 0.02%, $\delta^{15}N_{air} = +6.70 \pm 0.15$‰ (Elemental Microanalysis); and SDO-1, Devonian Ohio Shale, % TN = 0.36 ± 0.01%, $\delta^{15}N_{air} = -0.8 \pm 0.3$‰ (USGS). The data obtained were % TN = 0.14 ± 0.00% and $\delta^{15}N_{air}$ values of +6.76 ± 0.02‰ ($n = 3$) for B2153, and % TN = 0.37 ± 0.00% and −0.32 ± 0.02‰ ($n = 3$) for SDO-1.

Nano-elemental analyser-isotope ratio mass spectrometry analyses. A subset of extracted kerogens and bulk rock powders were also run for $\delta^{15}N$ by nano-elemental analyser-isotope ratio mass spectrometry at Syracuse University, following methods outlined in ref. 35. The benefit of this approach is that it is specifically designed for analysis of as little as 0.5 mg of kerogen and 50 nanomoles of N, thus limiting some of the complications associated with achieving complete combustion on larger samples. Encapsulated sample powders were evacuated to remove atmospheric N_2 present in capsule pore space and purged with Ar. Sample combustion was performed in an Elementar Isotope Cube elemental analyser with reaction conditions set at 1,100 °C and 650 °C for the oxidation and reduction reactors, respectively. Oxygen flow was set at 30 ml min^{-1} and introduced to the helium stream for 90 s, initiating when the sample is dropped into the oxidation reactor. The elemental analyser is coupled to an automated cryotrapping system that was built using a modified Elementar TraceGas analyser. The generated N_2 gas was trapped in a silica-gel-filled, stainless steel trap cooled in liquid N_2. Following complete collection of the N_2 peak from the high-flow elemental analyser, the He flow through the cryotrap was switched to a lower flow (2 ml min^{-1}) via actuation of a VICI Valco 6-port valve. The trap was heated and N_2 was released to a room-temperature capillary gas chromatography column (JW CarboBOND, 25 m, 0.53 mm internal diameter, 5 μm), and ultimately to the isotope ratio mass spectrometer. The Elementar elemental analyser traps CO_2 from combustion in a molecular sieve trap that is released to waste or to the isotope ratio mass spectrometer directly for $\delta^{13}C$ analyses. This ensures that CO_2 is not trapped in the N_2 cryotrap and mitigates the potential for neo-formed CO within the ion source. All samples were run in triplicate and blank-corrected using Keeling-style plots and normalized using the 2-point-correction scheme of ref. 34. Use of Keeling plots allows for simple estimation of the influence of the N_2 procedural blank on samples and for high-fidelity measurements of $\delta^{15}N$ on the small sample sizes employed. The reproducibility of replicate analyses of standards—IAEA N1 (0.4‰), IAEA N2 (+20.35‰) and NIST Peach Leaves (1.98‰)—and samples was ±0.26‰.

Additional analyses and data fidelity. Nitrogen is preserved in the sedimentary rock record primarily as organic N or as ammonium substituting for potassium in phyllosilicates[36]. The sedimentary N isotope values can be modified by a number of post-depositional processes, including diagenesis, burial and metamorphism. Therefore, before interpreting sedimentary $\delta^{15}N$ data, it is first necessary to examine the possible impacts of post-depositional alteration on the primary signal. Here we examine trends in supplementary and bulk rock data to validate our $\delta^{15}N$ dataset as representing a primary signal.

Degradation of organic matter during early diagenesis can offset primary $\delta^{15}N$ signals by 2‰ to 3‰ (ref. 37). High-pressure metamorphism does not impart significant $\delta^{15}N$ changes[38], although high-temperature metamorphism can increase $\delta^{15}N$ in ammoniated phyllosilicates (and possibly N_{org}; but see ref. 39) owing to volatilization of ^{15}N-depleted nitrogen[36,38]. Since the Rooihoogte and Timeball Hill formations have only experienced lower greenschist facies metamorphism[23], this mechanism would be expected to produce at most a 1‰–2‰ positive shift in $\delta^{15}N_{org}$. Cross-plots demonstrate no correlation between % N in kerogen (N_{org}) and $\delta^{15}N_{org}$ values (Extended Data Fig. 4a), rendering no evidence for metamorphic devolatilization of ^{15}N-depleted nitrogen from organics. $\delta^{15}N_{bulk}$ and % TN show only a loose positive correlation (with $R^2 = 0.34$; Extended Data Fig. 5a), in the opposite direction of what would be expected from substantial loss of ^{15}N-depleted N from whole rocks via devolatilization. Only a weak negative correlation exists between wt% TOC and $\delta^{13}C_{org}$ ($R^2 = 0.42$; Extended Data Fig. 4c), also inconsistent with substantial devolatilization of ^{13}C-depleted carbon during metamorphism. These data indicate that loss of N during metamorphism and deep burial did not greatly alter the primary $\delta^{15}N$ (or $\delta^{13}C$) values.

Nitrogen isotope exchange can occur between rocks and N-containing compounds when fluids migrate during organic matter maturation[40]. Similar to metamorphism, offset during thermal maturation generally results from preferential volatilization of ^{15}N-depleted nitrogen from organic molecules. The $\delta^{15}N$ of the natural gas is highly variable, but can have $\delta^{15}N$ as low[41,42] as −12‰. Nitrogen isotope exchange during fluid migration would tend to homogenize the isotopic composition of participating N pools, decreasing the isotopic range within the organic N pool and differences between organic and inorganic N pools[40]. Bulk rock $\delta^{15}N$ ($\delta^{15}N_{bulk}$) values cover the measured range of $\delta^{15}N_{org}$, but are generally more positive than $\delta^{15}N_{org}$, inconsistent with complete isotopic homogenization.

We observe only a very weak negative correlation between $\delta^{15}N_{bulk}$ and TOC:TN ($R^2 = 0.29$; Extended Data Fig. 5b), suggesting that some ^{15}N-enriched ammonium could have been sorbed onto and/or incorporated into clay minerals in very-low-TOC sediments, presumably during exchange with post-depositional fluids. The % TN (but not $\delta^{15}N_{bulk}$) indeed shows a clear positive correlation with % K_2O ($R^2 = 0.81$; Extended Data Fig. 5c), supporting incorporation of N into illites during K-metasomatism; however, there is no correlation between $\delta^{15}N_{bulk}$ and % K_2O ($R^2 = 0.10$; Extended Data Fig. 5d), suggesting that this exchange did not greatly affect bulk $\delta^{15}N$ values.

Data availability. Source Data for Fig. 2 and Extended Data Figs 4 and 5 are available in the online version of the paper. Data for Fig. 1 are from ref. 29 and references therein; full data table is available from the corresponding author on reasonable request.

31. Thomazo, C. & Papineau, D. Biogeochemical cycling of nitrogen on the early Earth. *Elements* **9,** 345–351 (2013).
32. Stüeken, E. E., Buick, R. & Schauer, A. J. Nitrogen isotope evidence for alkaline lakes on late Archean continents. *Earth Planet. Sci. Lett.* **411,** 1–10 (2015).
33. McKirdy, D. M. & Powell, T. G. Metamorphic alteration of carbon isotopic composition in ancient sedimentary organic matter: new evidence from Australia. *Geology* **2,** 591–595 (1974).
34. Coplen, T. B. *et al.* New guidelines for delta C-13 measurements. *Anal. Chem.* **78,** 2439–2441 (2006).
35. Polissar, P. J., Fulton, J. M., Junium, C. K., Turich, C. H. & Freeman, K. H. Measurement of ^{13}C and ^{15}N isotopic composition on nanomolar quantitites of C and N. *Anal. Chem.* **81,** 755–763 (2009).
36. Boyd, S. R. & Philippot, P. Precambrian ammonium biogeochemistry: a study of the Moine metasediments, Scotland. *Chem. Geol.* **144,** 257–268 (1998).
37. Robinson, R. S. *et al.* A review of nitrogen isotopic alteration in marine sediments. *Paleoceanography* **27,** http://dx.doi.org/10.1029/2012PA002321 (2012).
38. Bebout, G. E. & Fogel, M. L. Nitrogen-isotope compositions of metasedimentary rocks in the Catalina Schist, California: implications for metamorphic devolatilization history. *Geochim. Cosmochim. Acta* **56,** 2839–2849 (1992).
39. Ader, M., Boudou, J.-P., Javoy, M., Goffe, B. & Daniels, E. Isotope study of organic nitrogen of Westphalian anthracites from the Western Middle field of Pennsylvania (U.S.A.) and from the Bramsche Massif (Germany). *Org. Geochem.* **29,** 315–323 (1998).
40. Schimmelmann, A. & Lis, G. P. Nitrogen isotopic exchange during maturation of organic matter. *Org. Geochem.* **41,** 63–70 (2010).
41. Hoering, T. C. & Moore, H. E. The isotopic compositions of the nitrogen in natural gases and associated crude oils. *Geochim. Cosmochim. Acta* **13,** 225–232 (1958).
42. Murty, S. V. S. Noble-gases and nitrogen in natural gases from Gujarat, India. *Chem. Geol.* **94,** 229–240 (1992).
43. Sumner, D. Y. & Beukes, N. J. Sequence stratigraphic development of the Neoarchean Transvaal carbonate platform, Kaapvaal Craton, South Africa. *S. Afr. J. Geol.* **109,** 11–22 (2006).

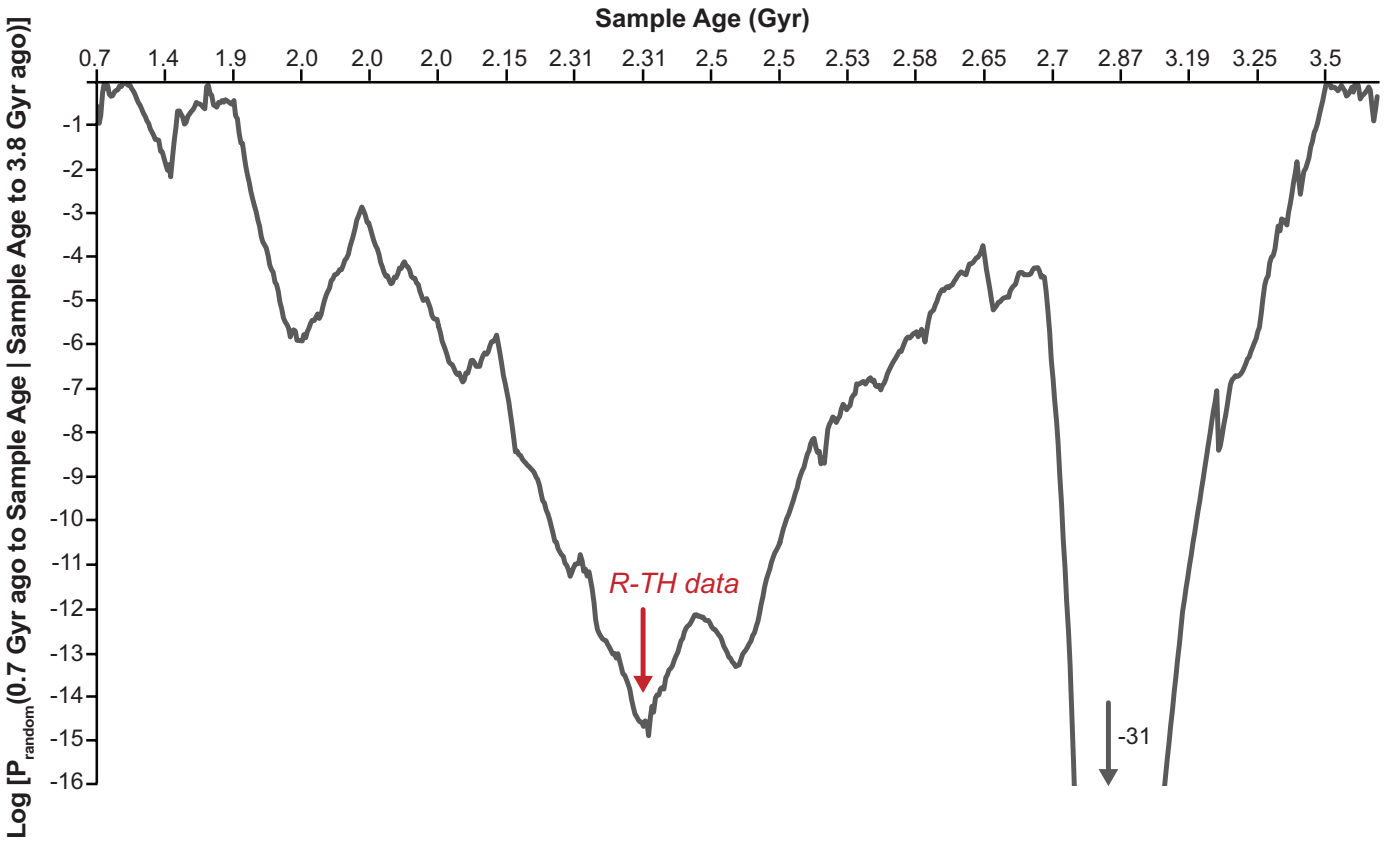

Extended Data Figure 1 | Results from statistical analysis of the $\delta^{15}N$ database. See Methods. 'R-TH' represents the Rooihoogte and Timeball Hill formations (this study). P_{random} is the 'false-positive' probability that the two sample sets separated by each pivot-age arise from populations of the same mean and variance. As discussed in the text, this value reaches an extreme of −31 when the sample sets are split into the time periods 0.70–2.71 Gyr ago and 2.75–3.80 Gyr ago (not shown).

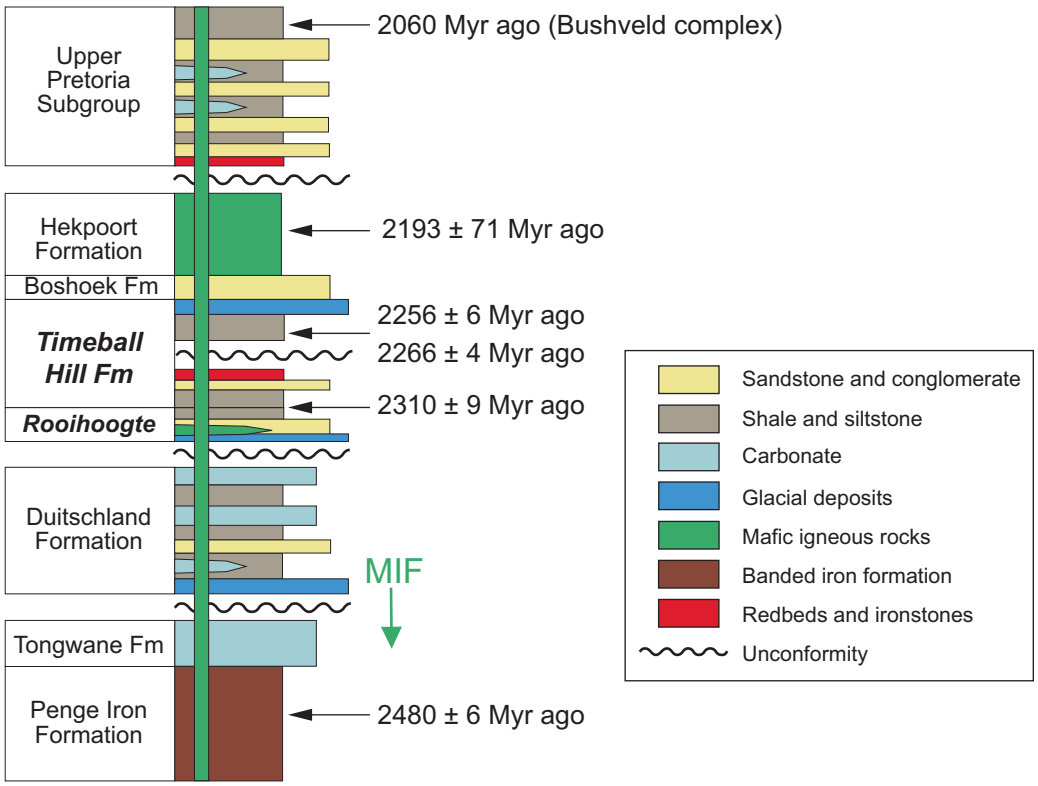

Extended Data Figure 2 | Stratigraphic context for the Rooihoogte and Timeball Hill formations within the Eastern Transvaal basin, South Africa, and associated ages. 'MIF' is the disappearance of the mass-independent fractionation of sulfur isotopes in the underlying Duitschland Formation (now known to reappear in the Rooihoogte Formation[6]). Fm, formation. Image adapted from ref. 5, Elsevier.

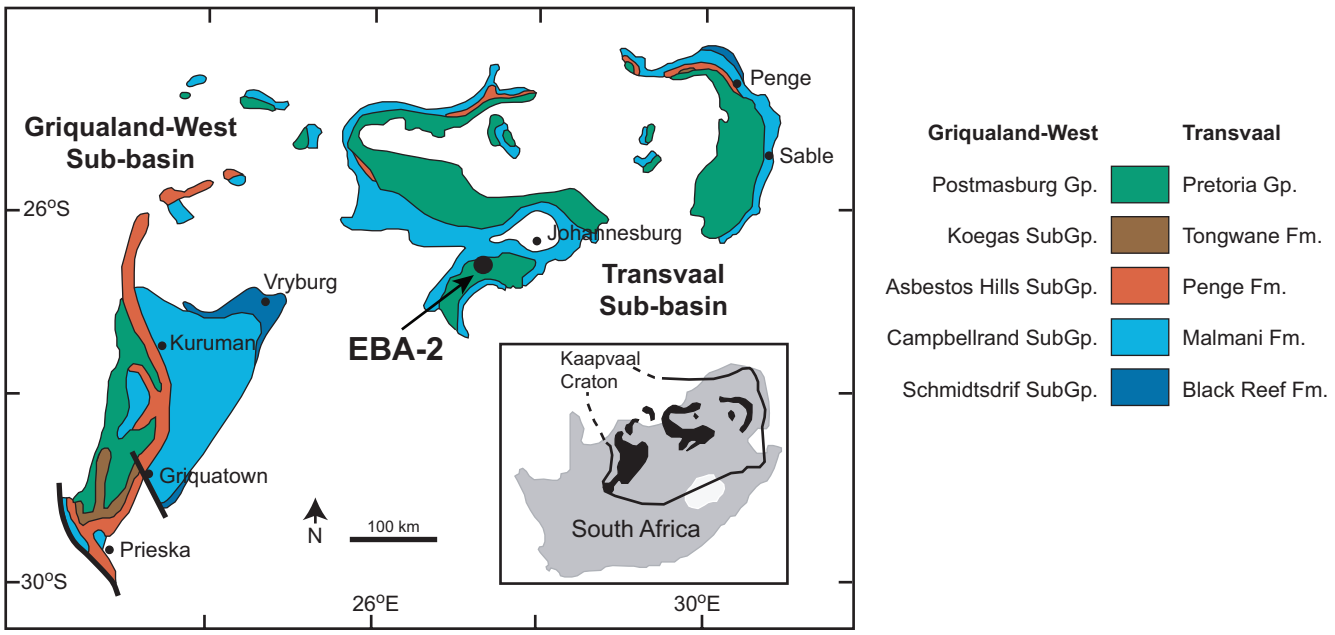

Extended Data Figure 3 | Simplified geologic map of the Transvaal Supergroup outcrop area. The location of drill core EBA-2 is shown. The core is currently stored at the National Core Library at Donkerhoek, which is managed by the Council for Geoscience in South Africa. Gp, group. Image adapted from ref. 43, Geological Society of South Africa.

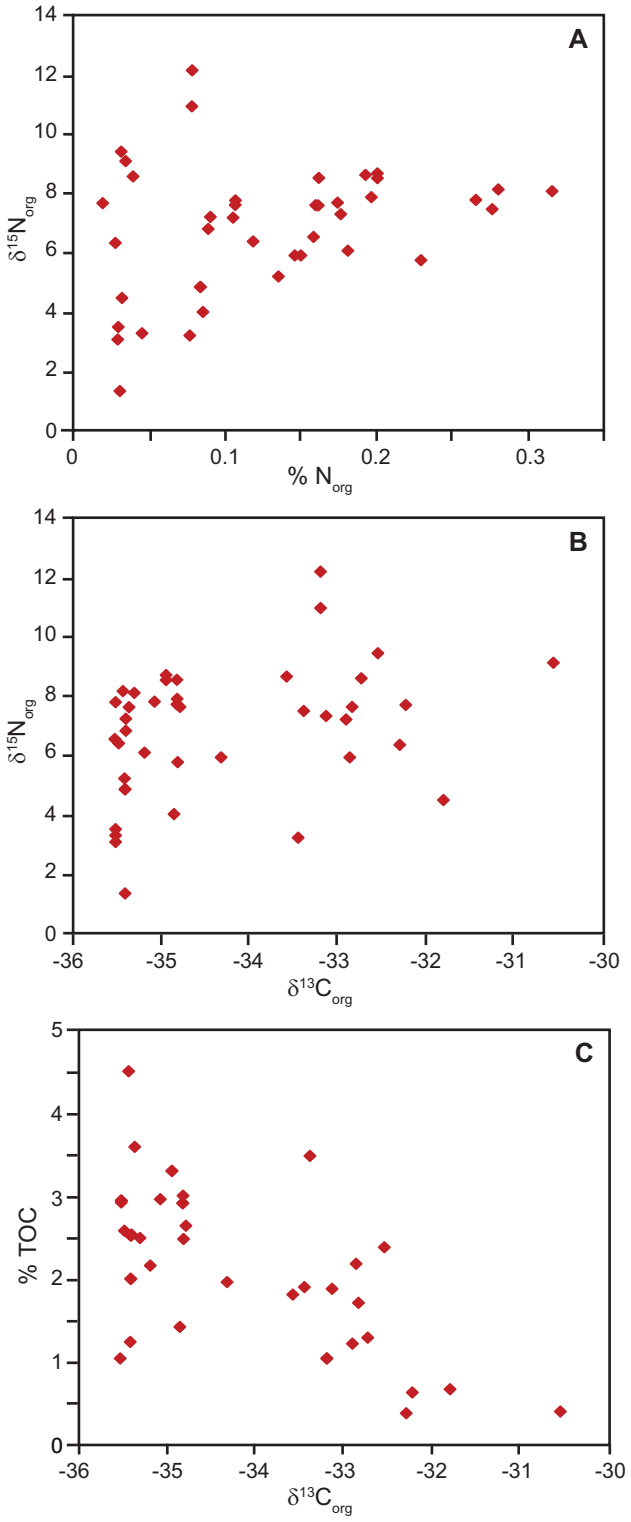

Extended Data Figure 4 | Additional data for kerogen analyses. **a**, Kerogen $\delta^{15}N$ ($\delta^{15}N_{org}$, in ‰) versus kerogen N abundance (% N_{org}). **b**, $\delta^{15}N_{org}$ versus organic $\delta^{13}C$ ($\delta^{13}C_{org}$, in ‰). **c**, Total organic carbon (% TOC) versus organic $\delta^{13}C$. For all data points, errors are within the size of the symbols.

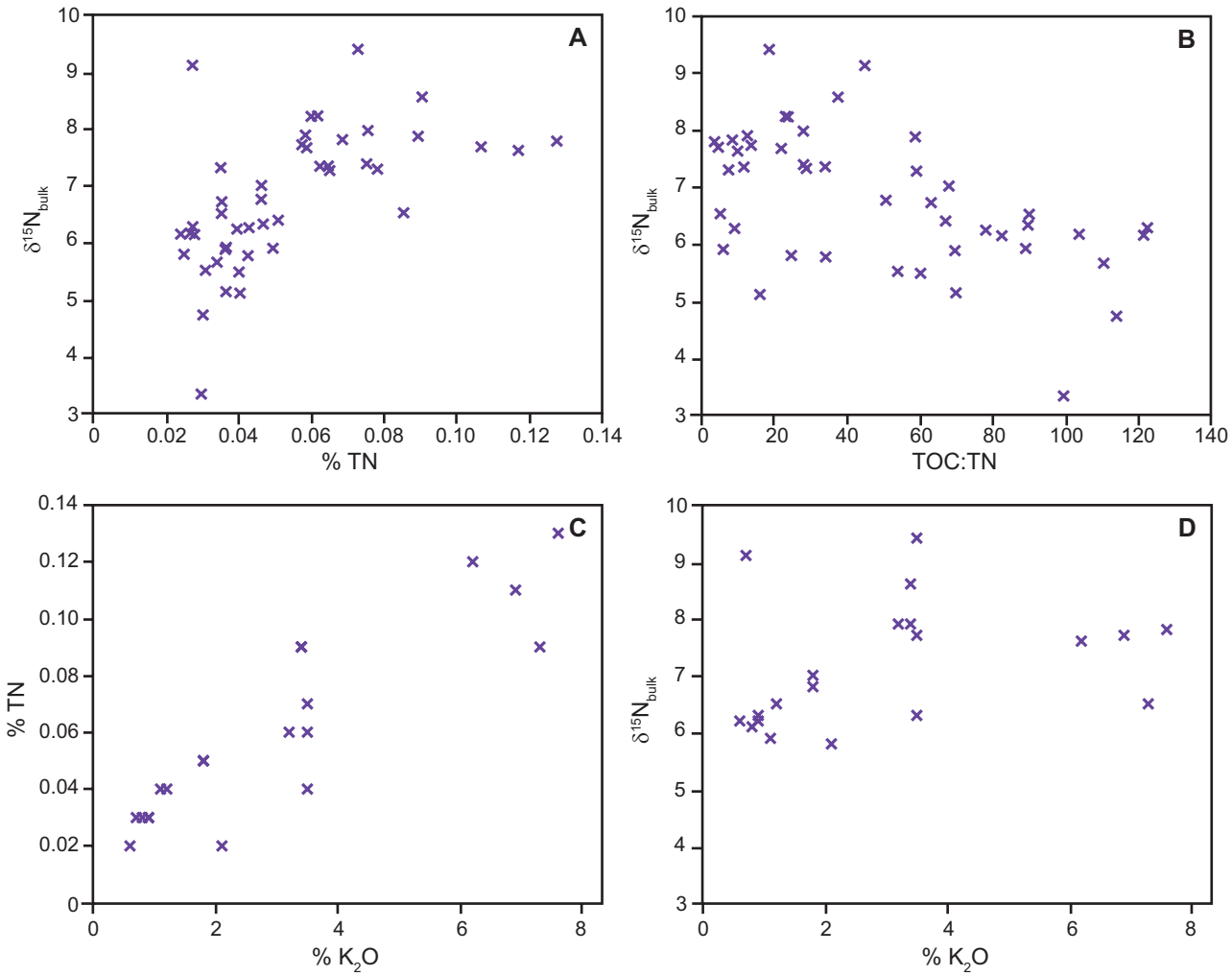

Extended Data Figure 5 | Additional data for bulk-rock analyses. a, Bulk-rock $\delta^{15}N$ ($\delta^{15}N_{bulk}$, in ‰) versus total nitrogen (% TN). **b**, $\delta^{15}N_{bulk}$ versus TOC:TN atomic ratios. **c**, % TN versus K_2O content (%). **d**, $\delta^{15}N_{bulk}$ versus K_2O content. For all data points, errors are within the size of the symbols.